

Plasma enhanced atomic layer deposition of molybdenum carbide and nitride with bis(tert-butylimido)bis(dimethylamido) molybdenum

Adam Bertuch Brent D. Keller, Nicola Ferralis, and Jeffrey C. Grossman Ganesh Sundaram

Citation: *Journal of Vacuum Science & Technology A: Vacuum, Surfaces, and Films* **35**, 01B141 (2017); doi: 10.1116/1.4972776

View online: <http://dx.doi.org/10.1116/1.4972776>

View Table of Contents: <http://avs.scitation.org/toc/jva/35/1>

Published by the [American Vacuum Society](#)

Articles you may be interested in

[Plasma-enhanced atomic layer deposition of superconducting niobium nitride](#)

Journal of Vacuum Science & Technology A: Vacuum, Surfaces, and Films **35**, 01B14301B143 (2016); 10.1116/1.4972858

[Stress modulation of titanium nitride thin films deposited using atomic layer deposition](#)

Journal of Vacuum Science & Technology A: Vacuum, Surfaces, and Films **35**, 01B14401B144 (2016); 10.1116/1.4972859

[Plasma enhanced atomic layer deposition of Al₂O₃ gate dielectric thin films on AlGaIn/GaN substrates: The role of surface predeposition treatments](#)

Journal of Vacuum Science & Technology A: Vacuum, Surfaces, and Films **35**, 01B14001B140 (2016); 10.1116/1.4972257

[Tris\(dimethylamido\)aluminum\(III\): An overlooked atomic layer deposition precursor](#)

Journal of Vacuum Science & Technology A: Vacuum, Surfaces, and Films **35**, 01B12801B128 (2016); 10.1116/1.4972469



Instruments for Advanced Science

Contact Hiden Analytical for further details:

W www.HidenAnalytical.com
E info@hiden.co.uk

[CLICK TO VIEW](#) our product catalogue



Gas Analysis

- › dynamic measurement of reaction gas streams
- › catalysis and thermal analysis
- › molecular beam studies
- › dissolved species probes
- › fermentation, environmental and ecological studies



Surface Science

- › UHV TPD
- › SIMS
- › end point detection in ion beam etch
- › elemental imaging - surface mapping



Plasma Diagnostics

- › plasma source characterization
- › etch and deposition process reaction
- › kinetic studies
- › analysis of neutral and radical species



Vacuum Analysis

- › partial pressure measurement and control of process gases
- › reactive sputter process control
- › vacuum diagnostics
- › vacuum coating process monitoring

Plasma enhanced atomic layer deposition of molybdenum carbide and nitride with bis(*tert*-butylimido)bis(dimethylamido) molybdenum

Adam Bertuch^{a)}

Ultratech-Cambridge NanoTech, Inc., 130 Turner Street, Waltham, Massachusetts 02453

Brent D. Keller, Nicola Ferralis, and Jeffrey C. Grossman

Department of Material Science and Engineering, Massachusetts Institute of Technology, 77 Massachusetts Ave., Cambridge, Massachusetts 02139

Ganesh Sundaram

Ultratech-Cambridge NanoTech, Inc., 130 Turner Street, Waltham, Massachusetts 02453

(Received 6 September 2016; accepted 8 December 2016; published 23 December 2016)

Molybdenum carbonitride films were deposited using plasma enhanced atomic layer deposition techniques with $(^t\text{BuN})_2(\text{NMe}_2)_2\text{Mo}$ at temperatures ranging from 80 to 300 °C. The elemental composition of the molybdenum carbonitride films were analyzed using x-ray photoelectron spectroscopy with a MoC_xN_y composition extending from carbide, $\text{MoC}_{0.45}\text{N}_{0.08}$ to nitride $\text{MoC}_{0.06}\text{N}_{1.40}$ (x : 0.06–0.45; y : 0.08–1.40). The film composition, electrical properties, and optical properties are strongly dependent upon the % N_2 in H_2 of the plasma gas stream, as well as the process temperature. The molybdenum carbide film ($\text{MoC}_{0.45}\text{N}_{0.08}$) deposited at 150 °C achieved an electrical resistivity (ρ) value of 170 $\mu\Omega\text{cm}$ and exhibited superconducting behavior with a transition temperature (T_c) of 8.8 K. Nitrogen rich molybdenum carbonitride films ($\text{MoC}_{0.28}\text{N}_{0.44}$) deposited at 250 °C with 6% N_2 in the plasma gas showed a microcrystalline fine grained structure with a measured $\rho = 200 \mu\Omega\text{cm}$. Film thickness and optical properties were characterized using spectroscopic ellipsometry with a measured growth per cycle extending from 0.36 to 0.56 Å/cycle. The measured optical properties extend across a broad range; refractive index (n : 3.1–3.4), and dielectric constant (k : 1.5–3.18). Grazing incidence x-ray diffraction of the MoC_xN_y films indicate a fine grained crystal structure, with a transition from a cubic MoC_{1-x} phase for the carbide to a face center cubic $\gamma\text{-Mo}_2\text{N}_{1+x}$ phase for the nitride films. © 2016 American Vacuum Society.

[<http://dx.doi.org/10.1116/1.4972776>]

I. INTRODUCTION

The interest in depositing thin films of molybdenum nitride and molybdenum carbide has increased due to the unique material properties associated with this transitional metal. Transition metal carbonitrides are closed packed metallic structures in which nitrogen and/or carbon atoms are interstitially located within the crystal structure, allowing for a wide range of material compositions, crystal structures, and interatomic bonding. Molybdenum carbides and nitrides are extremely hard, chemically stable, materials which make them good candidates for many mechanical applications. Their unique electrical properties and high catalytic activity suggests they may be an enabling material for fuel cells and catalytic applications. MoN_x has demonstrated superconductive behavior and also has low solubility to Cu with good electrical conductivity (200–500 $\mu\Omega\text{cm}$) making it a material of interest for diffusion barriers in Cu metallization applications.^{1,2}

Prior work has been demonstrated for depositing molybdenum nitride films using either atomic layer deposition (ALD) or plasma enhanced atomic layer deposition (PE-ALD) techniques at process temperatures >260 °C, with a wide range of reported ρ values (100–1500 $\mu\Omega$).^{3–6} Molybdenum carbide films have been deposited with techniques including

magnetron cosputtering⁷ and chemical vapor deposition (CVD) at temperatures >500 °C.^{8–10}

Molybdenum carbide is a transition metal carbide with superconducting properties, and demonstrated critical temperatures (T_c) extending from 5.1 to 12 K.^{11–14} Two-dimensional (2D) molybdenum carbide or nitride in a synthesized state with a surface termination group, called MXenes, exhibit either conducting or semiconducting properties and have been identified as potential thermoelectric materials. Synthesis and delimitation techniques have been demonstrated for 2D Mo_2C .¹⁵

The $(^t\text{BuN})_2(\text{NMe}_2)_2\text{Mo}$ molecule has been shown to be a viable avenue for depositing MoO_3 using either ozone or O_2 plasma as coreactants,^{16,17} and for depositing nitrides using NH_3 as an ALD coreactant.⁵ Molybdenum carbonitride films have been deposited using CVD at 450–650 °C with $\text{Mo}(\text{NBu}^t)_2(\text{NHBU}^t)_2$, a similar precursor molecule, where the film composition was reported as MoC_xN_y (x : 0.2–0.55, y : 0.1–0.47) as a function of deposition temperature and gas composition.⁹

In this study molybdenum carbonitride (MoC_xN_y) films were deposited using PE-ALD with $(^t\text{BuN})_2(\text{NMe}_2)_2\text{Mo}$ with a hydrogen/nitrogen plasma at temperatures from 80 to 300 °C with the goal of achieving high quality, electrically conductive films. At these relatively low deposition temperatures the electrical properties were characterized with ρ values ranging from 170 to 1500 $\mu\Omega\text{cm}$. As one would expect;

^{a)}Electronic mail: abertuch@ultratech.com

the resistivity, refractive index, and extinction coefficient of the deposited films are dependent upon the composition of the deposited carbonitride film. Film composition was determined using x-ray photoelectron spectroscopy (XPS), and grazing incidence x-ray diffraction (GIXRD) was used to identify the crystal structure. Further characterization was performed to explore the superconductive properties of the deposited molybdenum carbide film, and the crystallinity and surface morphology of the deposited MoC_xN_y was evaluated using atomic force microscopy (AFM).

II. EXPERIMENT

A. Atomic layer deposition

PE-ALD films were deposited in a top down flow, hot wall reactor, Ultratech Fiji G2 reactor. A remote inductively coupled plasma (ICP) source with 13.56 MHz and 300 W of power was used for the plasma process step. Samples were loaded and unloaded using a load lock chamber with sample cooling under vacuum conditions. The reactor temperature was maintained at a uniform process temperature for all deposited films with the chuck and wall temperatures controlled to the desired set point. The Ar gas flow for the ALD precursor delivery step was 30 sccm through the precursor manifold with 80 sccm of Ar into the plasma source.

The $(^t\text{BuN})_2(\text{NMe}_2)_2\text{Mo}$ precursor was heated to 60 °C and delivered to the chamber using an Ar boosted precursor delivery system to address the vapor pressure limitations of the molecule. The booster hardware delivers a reproducible Ar pulse to the precursor cylinder, increasing the pressure in the vapor headspace of the cylinder. After introducing the boost pulse of Ar, the precursor cylinder volume was pulsed into the chamber. For the Ar boost a 0.35 s pulse through a 100 μm flow restrictor was introduced into the 50 ml precursor cylinder, followed by a 0.5 s wait. After increasing the precursor delivery pressure, the $(^t\text{BuN})_2(\text{NMe}_2)_2\text{Mo}$ vapor space was pulsed at 0.75 s into the process chamber. This boost step was repeated three times with a 2 s wait for each precursor delivery step in the PE-ALD cycle, a total of three pulses per cycle.¹⁶ Other low vapor pressure delivery techniques could be employed, including direct liquid injection or a traditional bubbler design. The precursor delivery conditions were unchanged for all of the investigated deposition runs, and performed with nonturbo pumping on the reactor exhaust line, with a chamber pressure of 150 mTorr.

During the plasma process step, the Ar gas flows were reduced to 5 and 0 sccm to the ALD carrier and plasma source, respectively. Plasma process gas flows for each test condition were defined and stabilized before striking plasma with 300 W of power. Total plasma gas flow rates of 0–80 sccm were investigated with nitrogen concentrations, 0%–20% N_2 in H_2 . Turbo pumping was used for the entire plasma process step of the PE-ALD cycle to achieve chamber pressures in the 3–10 mTorr range, and allow for improved plasma coupling with the substrate. A 40 s plasma time with 5 s purge times between the plasma and precursor delivery steps was used for all investigated conditions.

B. Film analysis

Film thickness and optical parameters were measured using a Horiba Jobin Yvon, single angle, spectroscopic ellipsometry (SE) with a classical dispersion formula and a hybrid Lorentz and Drude model. Sample thickness was measured across a 200 mm wafer with a nine point cross pattern and an edge exclusion of 5 mm. Uniformity percent thickness of the film has been reported as (standard deviation)/average $\times 100$. Electrical resistivity measurements were performed at 10 Hz on a Stanford Research Systems SR830 using a standard AC lock-in method. The four point probe, pin contacts were made on 10 μm thick SiO_2/Si substrates at five locations across a 190 mm chamber diameter. Critical transition temperature measurements were carried out in a Quantum Design PPMS system with a base temperature of 2 K for superconductivity testing. Chemical composition and film purity was quantified using XPS. Survey scans were performed over regions 400 μm in diameter using a Thermo Scientific K-Alpha XPS with Aluminum $K\alpha$ radiation and processed with CASAXPS software for analysis and peak identification. Before spectral acquisition, the film surface was Ar sputtered for 2 min to remove surface oxide and reduce the impact of adventitious species. Shirley backgrounds and Gauss Lorentzian Product (90% Lorentzian weight) were used for peak deconvolution. GIXRD measurements were performed to evaluate the crystallinity and structure of the deposited films using a Rigaku SmartLab. Two theta (2θ) scans from 10° to 90° with a 1° angle of incidence from the source were collected. AFM was performed using a Veeco Metrology Nanoscope IV Scanned Probe Microscope Controller with Dimension 3100 SPM in tapping mode. PPP-NCHR probes with 7 nm radius of curvature were used, and roughness was calculated by averaging the measurements over a 25 μm square region.

III. RESULTS AND DISCUSSION

A. Uniformity and growth rate of MoC_xN_y

The plasma process step was optimized to achieve a complete forward reaction for the 11% N_2 in H_2 process. In Fig. 1, the plasma process time was investigate as a function of the measured response in the electrical resistivity (ρ), refractive index (n), and the dielectric constant (k), with the n and k values reported at a wavelength of 633 nm. The data suggest that a point of inflection is reached in the optical and electrical film properties at a plasma exposure time of ~ 15 s, beyond which n , k , and ρ remain constant and insensitive to the plasma exposure time. Therefore, for all subsequent experiments and reported data, a conservative 40 s plasma time was used.

The plasma process step was further investigated to quantify the impact of the $\text{N}_2:\text{H}_2$ plasma gas concentration (0%–20% N_2 in H_2) on the electrical and optical properties of the 150 °C deposited MoC_xN_y film (see Fig. 2). The measured resistivity of the MoC_xN_y film changes dramatically as a function of the N_2 concentration in the plasma gas, with values extending from 2000 $\mu\Omega\text{cm}$ for 20% N_2 in H_2 to

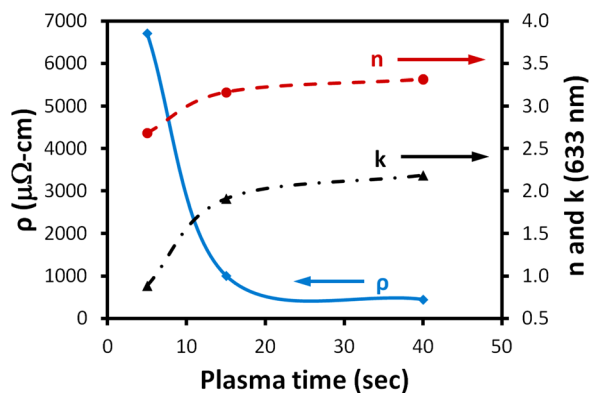


FIG. 1. (Color online) Resistivity, refractive index, and dielectric constant as a function of the plasma exposure time for 150 °C MoC_xN_y deposition with 11% N_2 in H_2 .

170 $\mu\Omega\text{cm}$ with a pure H_2 plasma gas concentration. A corresponding increase is observed in the dielectric constant as the resistivity decreases and the film becomes more electrically conductive. This relationship between ρ and k is not unexpected and is a useful method for inferring the electrical properties of the material using SE measured optical properties, n and k .

The growth per cycle (GPC) at 150 °C increases with higher N_2 concentrations for similar process conditions (Fig. 3). This suggests that increasing % N_2 in the plasma gas reduces the efficiency of the precursor ligand removal associated with the single and double bonded N, which is believed to be a function of the number of hydrogen and nitrogen radicals in the plasma at the wafer surface. The removal of N double bonds is critical for the formation of MoC_x and will be discussed in greater detail in Secs. III B 1 and III B 2. The thickness uniformity of the deposited films decreases as a function of N_2 concentration in the plasma gas, with the most uniform film achieved with 100% H_2 . In all cases investigated, the uniformity was <5% without process optimization.

The PE-ALD process using $(^t\text{BuN})_2(\text{NMe}_2)_2\text{Mo}$ with the 5.9% N_2 in H_2 , 40 s plasma was investigated for temperatures ranging from 80 to 300 °C, Fig. 4. Increasing the PE-ALD process temperature produces a measured decrease in the film's electrical resistivity with a corresponding increase

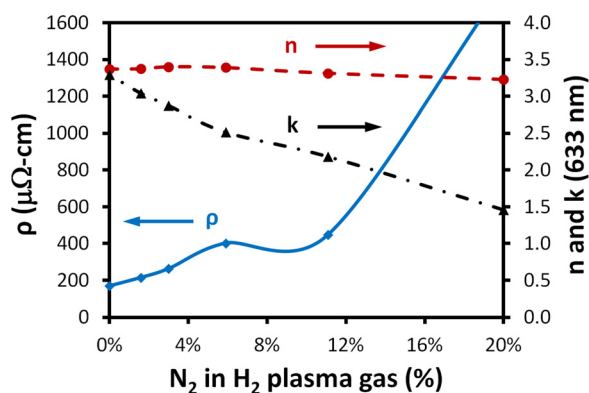


FIG. 2. (Color online) Electrical and optical properties for MoC_xN_y at 150 °C as a function of % N_2 in H_2 with 40 s, 300 W plasma.

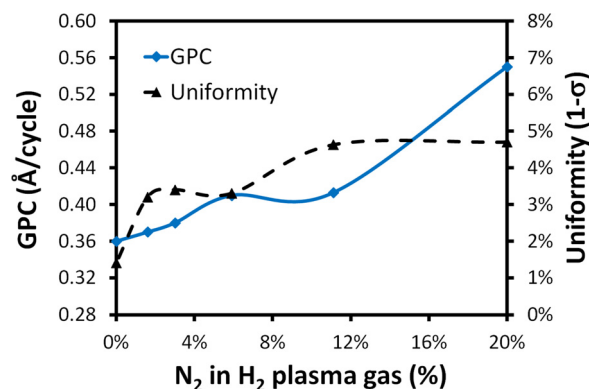


FIG. 3. (Color online) Growth per cycle and film thickness uniformity at 150 °C as a function of the % N_2 in H_2 plasma, with 40 s, 300 W plasma.

in the dielectric constant. At 250 °C, a ρ of 200 $\mu\Omega\text{cm}$ is achieved with a corresponding k (633 nm) value of 3.23. The refractive index at 633 nm increases modestly from 3.18 to 3.61 over the investigated temperature range, 80–250 °C. The 300 °C data are inconsistent with the trend observed at lower temperatures, and it is believed to be associated with a higher O_2 content in the film, as described by the lower k value. This increased O_2 component is observed in the XPS data and may be associated with an unexpected increase in oxygen concentration during the deposition.

From Figs. 2 and 4, one would expect that the trends associated with the changes in the plasma gas concentration (% N_2 in H_2) can be applied throughout the investigated process temperature range, producing similar trends for ρ , n , and k values. By selectively adjusting these recipe parameters, the MoC_xN_y properties and composition can be tuned to achieve the desired film properties for a specific application at either higher or lower process temperatures.

The growth per cycle as a function of temperature is reported in Fig. 5 where a plateau is observed at temperatures between 80 and 200 °C. The GPC increases fairly rapidly at temperatures above 200 °C, suggesting that the film growth mechanism may be increasing with the onset of precursor decomposition. A similar increases in GPC was observed when depositing MoO_3 with $(^t\text{BuN})_2(\text{NMe}_2)_2\text{Mo}$ with ozone using the same precursor delivery technique.¹⁶

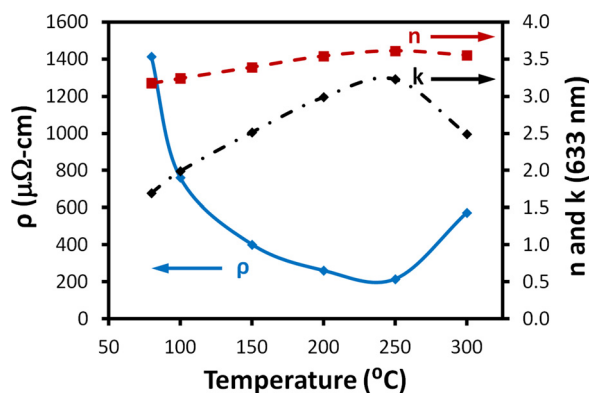


FIG. 4. (Color online) Electrical and optical properties as a function of deposition temperature with 5.9% N_2 in H_2 , 40 s, 300 W plasma.

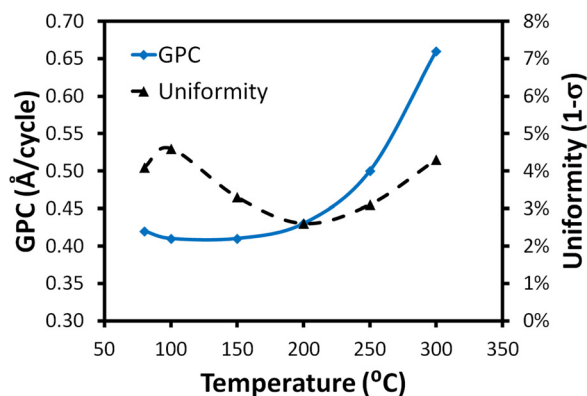


Fig. 5. (Color online) Growth per cycle and film thickness uniformity as a function of temperature with 5.9% N_2 in H_2 , 40 s, 300 W plasma.

B. Film characterization

1. X-ray photoelectron spectroscopy

XPS was used to identify the core level binding energies and oxidation state of the MoC_xN_y film and ultimately to evaluate the composition of the film. Within the sensitivity and threshold resolution of the XPS technique, the deposited films are composed of Mo, N, O, and C. The XPS spectral peaks were analyzed to determine the composition of deposited films with the results summarized in Figs. 6–11. The deconvolution of the N 1s and Mo $3p_{3/2}$ complex was used to evaluate the ratio of the N to Mo content (N:Mo) as has been performed for similar sputtered and pulsed laser deposited films (Fig. 6).¹ The atomic fractions of Mo, C, and O content were determined from the Mo 3d, C1s, and O1s peaks in a survey spectrum. The N content was then calculated from the N:Mo ratio.^{1,18}

The composition of the MoC_xN_y was evaluated for films deposited at 150 °C with 0%–20% N_2 in the H_2 plasma feed gas. Decreasing the plasma N_2 concentration yields a corresponding reduction in the N content in the film. As the N concentration decreases, the Mo and C concentration increase, and the O concentration is essentially unchanged. These data indicate a consistent transition from a molybdenum nitride film with a small carbon content to a molybdenum carbide

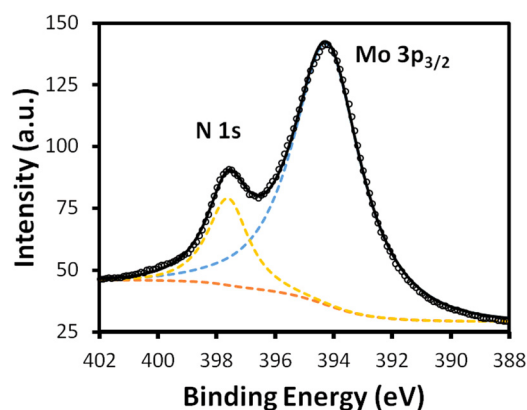


Fig. 6. (Color online) XPS peak deconvolution of N 1s and Mo $3p_{3/2}$ peaks for analysis of N and Mo film composition, 150 °C PE-ALD with 5.9% N_2 in H_2 .

film, with increasing H_2 plasma gas concentration, up to 100% H_2 . The atomic percentage of carbon and nitrogen appears to be essentially equal for the 150 °C deposition when the plasma gas concentration is $\sim 1.9\%$ N_2 in H_2 , and a film composition of $MoC_{0.33}N_{0.39}$.

Lowering the partial pressure of nitrogen in the plasma feed gas creates a hydrogen rich plasma with greater reducing power. The N double bonds in the precursor molecule are more difficult to remove than the single bonded N ligands and appear to have a higher probability of removal in the hydrogen radical rich plasma. The carbon content in the MoC_xN_y film is believed to originate from the $(^tBuN)_2(NMe_2)_2Mo$ precursor and becomes available for cross bridging during the 40 s H_2 rich plasma process step. Chiu *et al.* have proposed a β -methyl activation of the tertbutyl groups forming MeCN and HCN, followed by Mo-N bond disassociation as the mechanism for molybdenum carbonitride formation with a CVD process at temperatures $>300^\circ C$ with $Mo(NBu^t)_2(NHBU^t)_2$.⁹ This molecule has similar ligand groups to the precursor used in this study and their analysis may provide insight for the reaction mechanism observed in our plasma enhanced ALD process.

The 150 °C 100% H_2 plasma sample was evaluated for N concentration but the Auger N1s peak was below the threshold sensitivity of this technique, indicative of an N concentration <5 at. %, suggesting the film is MoC_x with a small nitrogen content. The XPS peaks for Mo, C, and O (shown on the left side of Fig. 7) were measurable, and assuming an N content of $\sim 5\%$, then the atomic composition of the film is $MoC_{0.45}N_{0.08}$.

Film composition as a function of temperature was evaluated with 5.9% N_2 in H_2 plasma gas for temperatures ranging from 80 to 300 °C (Fig. 8). Increasing process temperatures produced a decrease in the N content in the film up to 250 °C; similarly, the Mo and C concentration increase for this temperature range. Oxygen concentration decreases with increasing temperature consistently up to 250 °C, and increases for the 300 °C data.

For the test condition at 300 °C, both the oxygen and nitrogen concentration increase with a corresponding reduction in the carbon content. This transition in the film properties may be associated with precursor decomposition or due

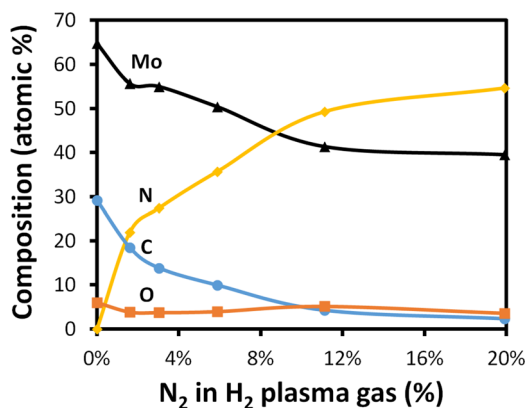


Fig. 7. (Color online) XPS compositional analysis of MoC_xN_y film as a function of % N_2 in H_2 , 150 °C PE-ALD process with 40 s, 300 W plasma.

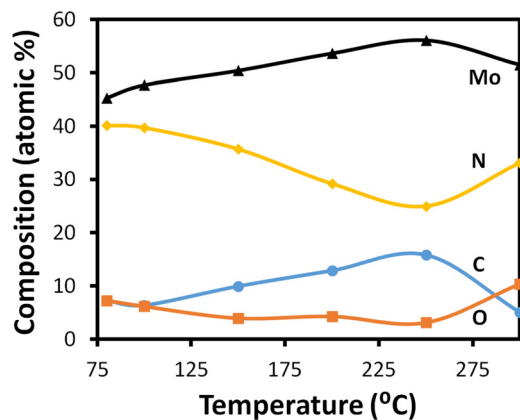


Fig. 8. (Color online) XPS compositional analysis of MoC_xN_y film as a function of deposition temperature using 5.9% N_2 in H_2 , 40 s, 300 W plasma process.

an elevated oxygen concentration associated with uncontrolled variables in the test reactor. Further investigation is required at temperatures greater than the 250°C to characterize this process space for the PE-ALD MoC_xN_y process.

In Fig. 9, the XPS data for MoC_xN_y films deposited at 150°C are summarized, and the composition extends from molybdenum carbide, $\text{MoC}_{0.45}\text{N}_{0.08}$, to a nitrogen rich molybdenum nitride, $\text{MoC}_{0.06}\text{N}_{1.4}$, as a function of the % N_2 in H_2 plasma gas. These data show that a full range of molybdenum carbonitride film compositions can be achieved by modifying the plasma process feed gas composition. For depositions with larger nitrogen plasma gas concentrations, films are nitrogen rich with an increasing interstitial concentration of N in the film, characteristic of a reduced plasma radical (H^*) concentration reaching the surface from the ICP remote plasma.

Film composition as a function of the deposition temperature was investigated, Fig. 10, with a fixed plasma process of 5.9% N_2 in the H_2 , 40 s, 300 W plasma. The carbide formation in the film increases with temperature, from 80 to 250°C , with both the C and N concentration defining linear behavior throughout this temperature range. The C content is essentially doubled while the N content is halved, showing a clear relationship between the carbon inclusion and nitrogen

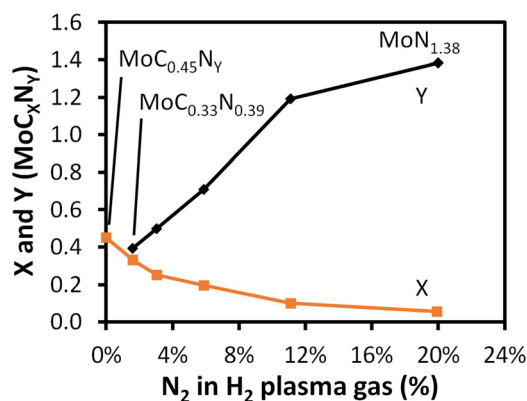


Fig. 9. (Color online) XPS composition of MoC_xN_y film as a function of % N_2 in H_2 with a 40 s, 300 W plasma process at 150°C .

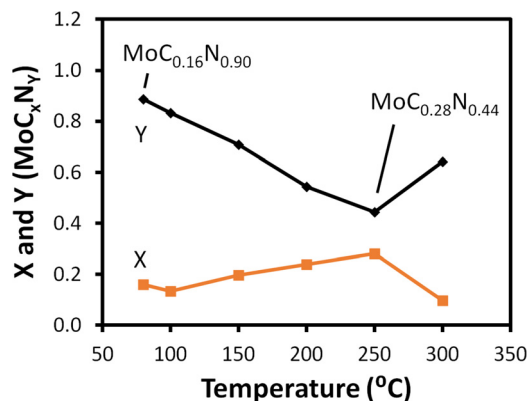


Fig. 10. (Color online) XPS composition of MoC_xN_y film as a function of process temperature using 5.9% N_2 in H_2 , 40 s, 300 W plasma process.

loss in the MoC_xN_y film as a function of temperature. The efficiency of the hydrogen rich, remote ICP plasma for removing the N bonded ligands in the precursor clearly increase with temperature for a fixed plasma condition, while also providing a carburizing environment for obtaining Mo–C bonds in the crystal structure.

At 300°C , the composition of the film trends to a nitrogen rich carbonitride with reduced carbon, supporting the conclusion of elevated oxygen content in the chamber for this condition.

Figure 11 shows XPS C1s spectra for carbon rich samples deposited at 150°C with 5.9% N_2 in H_2 and 100% H_2 plasma gas. XPS scans were performed before and after a 90 s Ar sputter clean, and observed peaks can be assigned to C–O, C–C, and C–Mo bonds located at 286.0, 284.6, and 283.3 eV. After removing the surface layer, the C–C peak at 284.6 eV is essentially undetectable in the spectra and one can clearly see the removal of adventitious and oxidized carbon located at the sample surface. The evidence of a clear C–Mo signal from the bulk material indicates that the carbon is primarily lattice bound in the crystal structure for the investigated conditions. Since there is no evidence of a C–C peak in the bulk material, it would indicate that there is very little aliphatic C in the film. Even though the hydrogen content has not been quantified in this study, these results

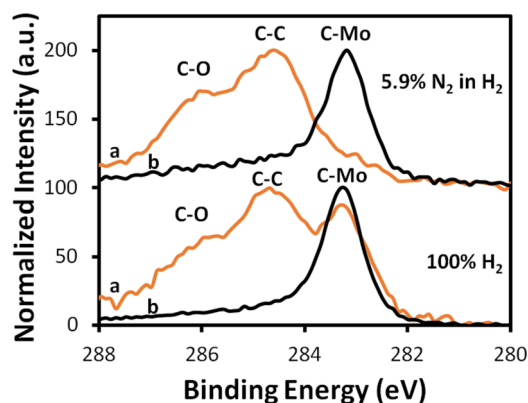


Fig. 11. (Color online) XPS spectra of the C1s peak for carbon rich films deposited at 150°C with 5.9% N_2 in H_2 , and 100% H_2 plasma gas, (a) before Ar sputter and (b) after 90 s Ar sputter.

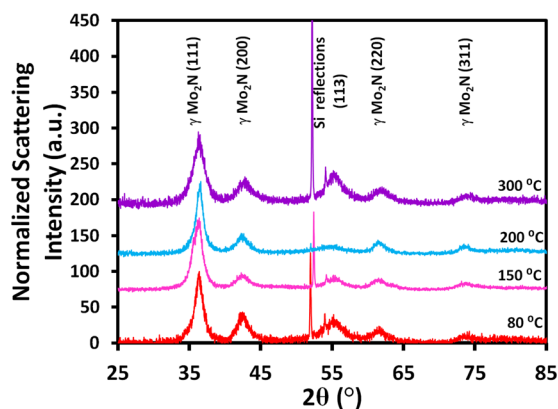


FIG. 12. (Color online) GIXRD survey scan for 5.9% N₂ in H₂ plasma gas for deposition at 80–300 °C.

suggest that the H₂ plasma environment removes the single and double bonded N from the chemisorbed organometallic precursor and provides a coreactant that produces a C-Mo bond in the resulting cubic structure.

2. Grazing incidence x-ray diffraction

GIXRD diffractograms were obtained to determine the crystallography of the samples. Depositions performed using 5.9% N₂ in H₂ plasma gas, Figs. 12 and 13, show well defined peaks for the γ -Mo₂N (111) and γ -Mo₂N (200) for all investigated temperatures, 80–300 °C. The GIXRD survey scan data have additional peaks characteristic of the cubic γ -Mo₂N with peaks observed at the γ -Mo₂N (220), and γ -Mo₂N (311) planes, Fig. 12. Additionally the silicon substrate Si (113) plane is observed in the survey scan with 2θ peaks at 52° and 55°.

Figure 13 shows the temperature dependence of the normalized (111) and (200) 2θ peaks. These peaks show very little variation in measured 2θ values as a function of temperature, 80–250 °C, yielding lattice constants for the (111) peak of 0.427–0.430 nm and the (200) peak of 0.424–0.428 nm, respectively.

The 250 °C sample with 5.9% N₂ plasma gas has a XPS measured composition of MoC_{0.28}N_{0.44}, and one would expect to see evidence of noncubic molybdenum carbide peaks in the GIXRD, if present in the film, but the crystallographic structure is unchanged with only a modest shift in the 2θ value suggesting that the carbon is either substitution or interstitial within the cubic structure.

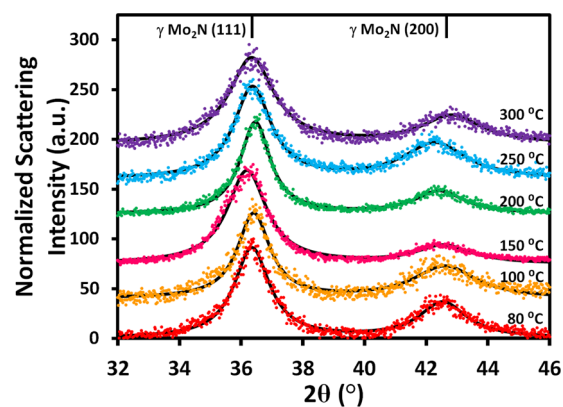


FIG. 13. (Color online) GIXRD data as a function of temperature with 5.9% N₂ in H₂ plasma gas. Solid lines indicate Lorentzian best fits.

GIXRD shows that the films deposited as a function of temperature with 5.9% N₂ in H₂ plasma gas are cubic γ -Mo₂N_{1±x} with characteristic 2θ peaks and lattice constants in agreement with data available in the literature.^{1,2}

The 2θ peak position, full width at half maximum (FWHM), and calculated lattice parameter data for the (111) and (200) peaks, as a function of deposition temperature, are summarized in Table I. The 300 °C diffractogram has wider peaks, as described by the larger FWHM values for both the (111) and (200) peaks and a reduced lattice constant for the (200) plane with a value of 0.422 nm, indicating a more dense crystal structure with greater long range disorder at this higher temperature. At 300 °C, the 2θ position for the (200) peak increases, suggesting a modest change in the crystal structure associated with the additional oxygen content of the film, complementing the observed trends in the XPS and SE results.

Diffractograms are available from the Joint Committee on Powder Diffraction Standards (JCPDS) for bulk, body centered tetragonal, β -Mo₂N_{0.78} (JCPDS, 25–1368) with peaks located at 37.8°, 43.2°, 45.2°, 62.6°, 64.2°, 75.5°, 78.2°, and 80.5°, which are assigned to the (111), (200), (002), (220), (202), (311), (113), and (222). The reflection peaks of cubic γ -Mo₂N from the JCPDS standard data (JCPDS, 25–1366) are 37.4°, 43.5°, 63.2°, 75.8°, and 79.8°, which correspond to (111), (200), (220), (311), and (222) reflections, respectively.^{19–21} Comparing our data with these standards show that we do not observe peaks associated with the (002), (202), and (113) planes of the tetragonal β -Mo₂N phase, in addition the peak height ratios that are consistent

TABLE I. GIXRD summary as a function of temperature with 5.9% N₂ in H₂ plasma gas.

T (°C)	XPS composition	(111) peak 2θ position (deg)	(111) FWHM (deg)	(200) peak 2θ position (deg)	(200) FWHM (deg)	(111) lattice constant a (nm)	(200) lattice constant a (nm)
80	MoC _{0.16} N _{0.89}	36.34	1.40	42.53	1.88	0.428	0.425
100	MoC _{0.13} N _{0.83}	36.40	1.27	42.60	2.47	0.428	0.424
150	MoC _{0.20} N _{0.71}	36.18	1.54	42.55	2.14	0.430	0.425
200	MoC _{0.24} N _{0.54}	36.45	1.19	42.42	1.98	0.427	0.426
250	MoC _{0.28} N _{0.44}	36.36	1.46	42.28	2.45	0.428	0.428
300	MoC _{0.10} N _{0.64}	36.33	1.77	42.83	2.37	0.428	0.422

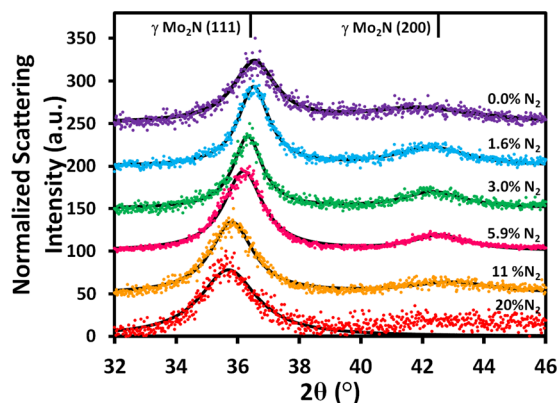


FIG. 14. (Color online) GIXRD data as a function of plasma gas concentration, 0%–20% N_2 in H_2 , at 150 °C. Solid lines indicate Lorentzian best fits.

with the γ - $Mo_2N_{1\pm x}$ phase. The molybdenum nitride structure is believed to be a NaCl type crystal with a cubic array of Mo atoms with N atoms randomly occupying half of the octahedral interstices.² The MoC_xN_y films exhibit well defined diffraction peaks for a cubic structure of γ - $Mo_2N_{1\pm x}$ with a carbide component of cubic MoC.

Miikkulainen *et al.* investigated a thermal ALD process for MoN, using the same precursor ($tBuN$)₂(NMe)₂Mo with NH_3 gas as the coreactant at 260–300 °C, and reported an amorphous film containing small amounts of the β - Mo_2N phase.⁵ The reported difference in material structure may be attributed to the more energetic $N_2:H_2$ plasma coreactant used in this study developing the γ - $Mo_2N_{1\pm x}$ phase, which is typically produced at higher temperatures. Due to the close proximity of the (111), (200), (220), and (311) 2- θ peaks, it is possible that the body centered tetragonal β - MoN_2 is also present with the γ - MoN_2 phase. However, if the β phase is present in significant quantities, the β - Mo_2N peaks associated with the (002), (202), and (113) planes would be expected in diffractograms. For this reason, we believe the synthesized films are predominantly γ - $Mo_2N_{1\pm x}$. The measured lattice constants appear to be consistent with reported values for deposited films of γ - Mo_2N , albeit at the higher end of the reported window, this is believed to be associated with the elevated concentration of interstitial C and N in the films.²

The molybdenum carbide system has a number of crystal structures as reported in the literature, α - MoC_{1-x} , δ - MoC , β - Mo_2C , η - MoC , γ - MoC , etc.^{7–11} This is a complicated material system with numerous variations and in some cases conflicting information. The α - MoC_{1-x} and δ - $MoC_{0.67}$

phases have been reported as face centered cubic, NaCl type, crystal with an ABCABC stacking sequence. The peaks observed in our data are consistent with the reported cubic crystal structure of α - MoC_{1-x} and the δ - MoC_{1-x} with characteristic 2 θ peak positions and peak heights.^{7,9,21} The hexagonal crystal structures, for example, β - Mo_2C , have characteristic 2 θ peaks at 34.5°, 38.0°, 39.5°, 52.5°, 63°, 69.8°, and 74.8°.^{22,23} In our GIXRD data for the carbide rich material, we do not see evidence for other crystallographic structures, suggesting that the material is predominantly a cubic MoC_xN_y .

GIXRD data at 150 °C with various plasma gas concentrations, 0%–20% N_2 in H_2 , are presented in Fig. 14 and summarized in Table II. Depositions with N_2 concentrations >6% in hydrogen produce films with less long range order, as can be seen for the 20% N_2 case where the (200) peak is not observed. As the N_2 concentration decreases, the carbon content in the film and the γ - $Mo_2N_{1\pm x}$ (111) 2 θ peak value increases, suggesting that the film transitions from a cubic nitride to a cubic carbide, with the film becoming more dense as described by the smaller measured lattice parameters. This shift is expected as less interstitial N is included in the crystal structure and as smaller C atom replaces N in the lattice forming a carbon rich substitutional MoC_xN_y . In addition, the plasma with reduced % N_2 in the H_2 gas describes taller narrower peaks indicating greater order in the crystal structure and larger microcrystallinity. During the transition from high nitrogen concentrations, 20%–3.0% N_2 in H_2 plasma gas, the (111) FWHM value decreases, suggesting a reduction in the grain size, with a minima at 3.0% N_2 . This minima in the (111) FWHM occurs at the $MoC_{0.25}N_{0.50}$ composition near the nominal Mo_2N stoichiometry, suggesting that the contraction in the lattice constant is associated with the removal of interstitial N.

From the GIXRD data, it is believed that as the film transitions from a nitride to carbide, at <3.0% N_2 in H_2 plasma gas, the carbon located on the lattice forms the cubic α - MoC_{1-x} structure with a modest further reduction in the measured lattice constant. As the plasma gas concentration reaches 100% H_2 , the α - MoC_{1-x} crystal size increases as indicated by an increase in the (111) FWHM value. With a composition of $MoC_{0.45}N_{0.08}$, the lattice constant was calculated to be 0.426 nm, a value consistent with higher carbon in the carbide films, as reported by Lu *et al.* for a 800 °C CVD deposited cubic $MoC_{0.67}$ (40 at. % C).⁸ Using the Scherrer formula with the (111) peak 2 θ and FWHM values,

TABLE II. GIXRD summary as a function of plasma gas concentration for depositions at 150 °C.

% N_2 in H_2 plasma gas	XPS composition	(111) peak 2 θ position (deg)	(111) FWHM (deg)	(200) peak 2 θ position (deg)	(200) FWHM (deg)	(111) lattice constant a (nm)	(200) lattice constant a (nm)
20.0%	$MoC_{0.06}N_{1.38}$	35.69	2.26			0.436	
11.1%	$MoC_{0.10}N_{1.19}$	35.80	1.67	42.93	3.42	0.434	0.421
5.9%	$MoC_{0.20}N_{0.71}$	36.18	1.54	42.55	2.14	0.430	0.425
3.0%	$MoC_{0.25}N_{0.50}$	36.32	1.16	42.34	2.42	0.428	0.427
1.6%	$MoC_{0.33}N_{0.39}$	36.51	1.21	42.28	2.77	0.426	0.428
0.0%	$MoC_{0.45}N_{0.08}$	36.53	1.67	41.89	4.64	0.426	0.431

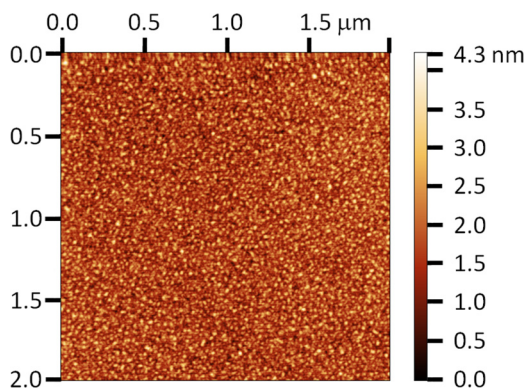


Fig. 15. (Color online) AFM image of 150 °C PE-ALD deposition with 5.9% N₂ in H₂, 40 s, 300 W plasma.

the average grain diameter was calculated to be 40–75 Å for the investigated process range, characteristic of a fine grained microstructure.

3. Atomic force microscopy

AFM was used to characterize the surface morphology and crystal size of the PE-ALD molybdenum carbonitride, a 16 nm thick MoC_{0.20}N_{0.71} sample deposited at 150 °C with 5.9% N₂ in H₂, 40 s, 300 W plasma was investigated. The average roughness (R_a) and root mean square roughness (R_{RMS}) were measured for the film, yielding a $R_a = 3.39 \pm 0.44$ Å and $R_{RMS} = 4.30$ Å, Fig. 15. The RMS roughness is 2.7% of the film thickness, indicating a fine grained microstructure with a smooth, uniform distribution of crystallites across the surface.

4. Superconductivity of MoC_x

Superconductivity was investigated for the cubic molybdenum carbide film deposited at 150 °C with the 100% H₂, 40 s plasma process. The 15 nm thick sample was investigated due to its low measured ρ value at room temperature, 170 $\mu\Omega$ cm, suggesting that it may be a good candidate for superconductive behavior. The molybdenum carbide thin film with an XPS determined stoichiometry of MoC_{0.45}N_{0.08} demonstrated superconducting behavior with a transition temperature (T_c) at 8.8 K (see Fig. 16).

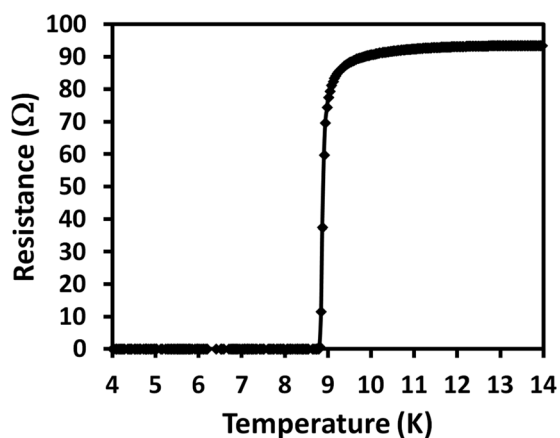


Fig. 16. Superconductivity measurement of 150 °C PE-ALD deposition with 100% H₂, 40 s, 300 W plasma.

From the literature, superconducting δ -MoC_{0.681} cubic Mo carbide has been measured with a $T_c = 12$ K, where the material was synthesized from stoichiometric carbon and Mo powder using high-pressure, 6 GPa, to create a material with numerous disordered, carbon vacancies in the cubic host structure.²⁴ Hexagonal-layered η -Mo₃C₂ superconductors have been fabricated from powders pressed in a 6 GPa 1700 °C furnace, yielding a $T_c = 8.5$ K.¹¹ Also, molybdenum carbide films have demonstrated superconductive behavior with reported T_c values from 5.1 to 8.9 K for α -Mo₂C and β -Mo₂C phase materials.¹² The highest reported T_c for molybdenum carbide is for a single-cubic δ -MoC_{1-x} with a transition temperature of 14.7 K using an arc melting solidification technique with a film composition of MoC_{0.65} to MoC_{0.75}.¹⁴

Our results are within the range of reported values and provide a new technique for depositing thin superconducting molybdenum carbide films at comparably low process temperatures, 150 °C.

IV. SUMMARY AND CONCLUSIONS

PE-ALD of molybdenum carbonitride films were investigated using (tBuN)₂(NMe₂)₂Mo and N₂:H₂ plasma for temperatures ranging from 80 to 300 °C. The film composition, electrical resistivity (ρ), and optical properties (n and k) of the films are strongly dependent upon the deposition temperature and % N₂ in the H₂ plasma gas. Molybdenum carbide and nitride films were deposited with an elemental composition of the MoC_xN_y extending from (x : 0.45–0.06; y : 0.08–1.4). At 150 °C, the % N₂ in the H₂ plasma gas directly impacts the N and C composition in the molybdenum film, as well as the n , k , and ρ values of the film. The molybdenum carbide film deposited at 150 °C with 100% H₂, yielded measured $n = 3.3$, $k = 3.3$, $\rho = 170 \mu\Omega$ cm values, and also exhibits superconducting properties with a $T_c = 8.8$ K.

The growth per cycle for the investigated process extends from 0.36 to 0.56 Å/cycle at 150 °C as a function of the N₂% in the H₂ plasma gas with thickness uniformity across a 200 mm wafer <5% (1- θ) for all investigated conditions.

The MoC_xN_y depositions have a fine grained cubic crystal microstructure with a grain size = 58 ± 18 Å, and an $R_{RMS} = 4.30$ Å. The nitrogen rich films are primarily γ -Mo₂N_{1±x} phase face centered cubic with a transition to a face centered cubic MoC_x as the N content decreases to <5% in the plasma process gas.

ACKNOWLEDGMENT

The authors would like to thank Yonas Yemane from Stanford University for providing the superconductivity measurements.

¹Y. Wang and R. Lin, *Mater. Sci. Eng., B* **112**, 42 (2004).

²I. Jauberteau, A. Bessaudou, R. Mayet, J. Cornette, J. L. Jauberteau, P. Carles, and T. Merle-Mejean, *Coatings* **5**, 656 (2015).

³P. Alen, M. Ritala, K. Arstila, J. Keinonen, and M. Leskela, *J. Electrochem. Soc.* **152**, G361 (2005).

⁴D. K. Nandi, U. K. Sen, D. Choudhury, S. Mitra, and S. K. Sarkar, *ACS Appl. Mater. Interfaces* **6**, 6606 (2014).

- ⁵V. Miikkulainen, M. Suvanto, and T. A. Pakkanen, *Chem. Mater.* **19**, 263 (2007).
- ⁶Y. Jang, J. B. Kim, T. E. Hong, and S. Kim, *J. Alloy Compd.* **663**, 651 (2015).
- ⁷G. De Temmerman, M. Ley, J. Boudaden, and P. Oelhafen, *J. Nucl. Mater.* **337–339**, 956 (2005).
- ⁸J. Lu, H. Hugosson, O. Eriksson, L. Nordstrom, and U. Jansson, *Thin Solid Films* **370**, 203 (2000).
- ⁹H.-T. Chiu, W.-Y. Ho, and S.-H. Chuang, *J. Mater. Res.* **9**, 1622 (1994).
- ¹⁰T. Nakajima and T. Shirasaki, *J. Electrochem. Soc.* **144**, 2096 (1997).
- ¹¹K. Yamaura, Q. Huang, M. Akaishi, and E. Takayama-Muromachi, *Phys. Rev. B* **74**, 184510 (2006).
- ¹²M. K. Kolel-Veetil, S. B. Qadri, M. Osofsky, and T. M. Keller, *Chem. Mater.* **17**, 6101 (2005).
- ¹³Z. H. Wang, L. Di, D. Y. Geng, S. Ma, W. Liu, and Z. D. Zhang, *Phys. Status Solidi* **205**, 2919 (2008).
- ¹⁴N. S. Athanasiou, *Mod. Phys. Lett. B* **11**, 939 (1997).
- ¹⁵J. Halim *et al.*, *Adv. Funct. Mater.* **26**, 3118 (2016).
- ¹⁶A. Bertuch, G. Sundaram, M. Saly, D. Moser, and R. Kanjolia, *J. Vac. Sci. Technol., A* **32**, 01A119 (2014).
- ¹⁷M. F. J. Vos, B. Macco, N. F. W. Thissen, A. A. Bol, and W. M. M. Kessels, *J. Vac. Sci. Technol., A* **34**, 01A103 (2016).
- ¹⁸S. Gong, H. Chen, W. Li, and B. Li, *Appl. Catal. A* **279**, 257 (2005).
- ¹⁹F. Cardenas-Lizana, S. Gomez-Quero, N. Perret, L. Kiwi-Minsker, and M. A. Keane, *Catal. Sci. Technol.* **1**, 794 (2011).
- ²⁰C. Wan, Y. Regmi, and B. M. Leonard, *Angew. Chem.* **126**, 6525 (2014).
- ²¹K. Inumaru, K. Baba, and S. Yamanaka, *Physica B* **383**, 84 (2006).
- ²²L. Cunha, L. Rebouta, F. Vaz, and J. P. Riviere, *Vacuum* **82**, 1428 (2008).
- ²³C. Liu, M. Lin, K. Fang, Y. Meng, and Y. Sun, *RSC Adv.* **4**, 20948 (2014).
- ²⁴C. I. Sathish *et al.*, *J. Solid State Chem.* **196**, 579 (2012).